



In vitro real-time magnetic resonance imaging for quantification of thrombosis

Ling Yang¹ · Thomas Neuberger^{1,2} · Keefe B. Manning^{1,3}

Received: 26 February 2020 / Revised: 20 July 2020 / Accepted: 22 July 2020 / Published online: 29 July 2020
© European Society for Magnetic Resonance in Medicine and Biology (ESMRMB) 2020

Abstract

Objectives Thrombosis is a leading cause of failure for cardiovascular devices. While computational simulations are a powerful tool to predict thrombosis and evaluate the risk for medical devices, limited experimental data are available to validate the simulations. The aim of the current study is to provide experimental data of a growing thrombus for device-induced thrombosis.

Materials and methods Thrombosis within a backward-facing step (BFS), or sudden expansion was investigated, using bovine and human blood circulated through the BFS model for 30 min, with a constant inflow rate of 0.76 L/min. Real-time three-dimensional flow-compensated magnetic resonance imaging (MRI), supported with Magnevist, a contrast agent improving thrombus delineation, was applied to quantify thrombus deposition and growth within the model.

Results The study showed that the BFS model induced a flow recirculation region, which facilitated thrombosis. By 30 min, in comparison to bovine blood, human blood resulted in smaller thrombus formation, in terms of the length (13.3 ± 0.6 vs. 18.1 ± 1.3 mm), height (2.3 ± 0.1 vs. 2.6 ± 0.04 mm), surface area exposed to blood (0.67 ± 0.03 vs. 1.05 ± 0.08 cm²), and volume (0.069 ± 0.004 vs. 0.093 ± 0.007 cm³), with $p < 0.01$. Normalization of the thrombus measurements, which excluded the flow recirculation effects, suggested that the thrombus sizes increased during the first 15 min and stabilized after 20 min. Blood properties, including viscosity, hematocrit, and platelet count affected thrombosis.

Conclusion For the first time, contrast agent-supported real-time MRI was performed to investigate thrombus deposition and growth within a sudden expansion. This study provides experimental data for device-induced thrombosis, which is valuable for validation of computational thrombosis simulations.

Keywords Thrombosis · Magnetic resonance imaging · Computational fluid dynamics

Introduction

Cardiovascular disease is the number one cause of death in the United States. In 2017, about 92.1 million adults suffered from some form of the disease including heart failure, coronary heart disease, and stroke [1]. For the patients in severe stages, implantation of cardiovascular devices is an effective treatment. However, thrombosis remains a challenging

obstacle for these devices to interact with blood and operate flawlessly. Device-induced thrombosis often causes device malfunctioning and embolization of the thrombus into the circulatory system, which can block a downstream artery, leading to further complications. Studies have reported that occurrences of thrombosis in heart pumps and prosthetic valves reduce the survival rate of patients by up to 50% [2, 3]. To minimize the risk of thrombosis in cardiovascular devices, it is necessary to understand the underlying mechanisms.

The hemodynamics of blood flow and biochemical reactions affect thrombus formation in the circulatory system. While endothelial injury is a typical condition that triggers thrombosis, device-induced thrombosis oftentimes results from interaction between blood, a foreign surface, and irregular geometry, which induces abnormal shear distribution within the flow. In hemostasis, most platelets in

✉ Keefe B. Manning
kbn10@psu.edu

¹ Department of Biomedical Engineering, The Pennsylvania State University, University Park, PA, USA

² Huck Institutes of Life Science, The Pennsylvania State University, University Park, PA, USA

³ Department of Surgery, Penn State Hershey Medical Center, Hershey, PA, USA

the circulation are non-activated. However, when the platelets are exposed to high shear stresses ($> 10 \text{ dyn/cm}^2$) for sufficient time, they become activated and more adhesive [4]. The activated platelets tend to aggregate and deposit on surfaces with low wall shear rate ($< 500 \text{ s}^{-1}$), releasing chemical elements to amplify platelet activation and chemical factors to trigger the coagulation cascade, via the intrinsic or extrinsic pathway [5]. The intrinsic coagulation pathway occurs when blood is in contact with a foreign surface, where contact activation of factor XII is involved [6]; while, the extrinsic pathway is in response to tissue injury. Both pathways lead to activation of thrombin and formation of a fibrin mesh. The cross-linked fibrin polymers stabilize the platelet aggregates and result in a formed thrombus.

The enhanced computational power and better knowledge of the thrombotic process make numerical simulations of device-induced thrombosis possible, becoming a powerful tool for evaluating the effects of hemodynamic and biochemical factors on thrombosis. Recent studies have shown that numerical simulations for thrombosis can help optimize the implantation of stents [7], flow diverters [8], and ventricular assist devices [9, 10], with lower risk of thrombosis. Multiple numerical models have been developed to simulate thrombosis [11–16]. However, limited experimental data are available for model validation.

Magnetic resonance imaging (MRI) is a useful technique for thrombus detection in clinical and laboratory settings [17–19]. For device-induced thrombosis, Taylor et al. [20] performed in vitro MRI studies to quantify thrombus deposition and growth within a backward facing step (BFS) model. Due to the presence of a sudden expansion within the model,

flow recirculation was induced while blood flowed through the model, which promoted thrombosis at the step region. During the experiment, bovine blood was recirculated through the BFS model and a thrombus was allowed to grow for a specified time. Once a particular time was reached, the blood was replaced with phosphate-buffered saline (PBS) to image the thrombus. Taylor et al. [20] provided quantitative measurements for thrombus deposition and growth within a device over time. As the thrombus has similar T1 values compared to blood ($1943 \pm 50 \text{ ms}$ vs. $1949 \pm 5 \text{ ms}$; at 7 T), it was imaged against stationary PBS, instead of flowing blood. Consequently, the resultant thrombus quantification and topology were affected.

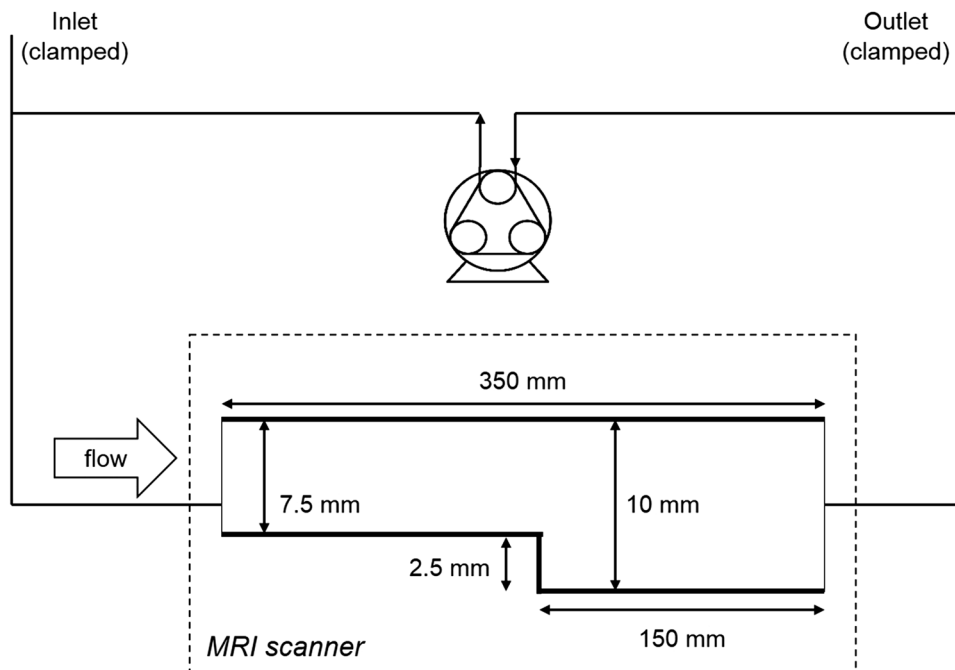
To better understand the effects of hemodynamics on device-induced thrombosis and to provide more accurate experimental data for thrombosis computational model validation, in vitro three-dimensional flow-compensated MRI experiments were performed in this study. Continuous application of Magnevist (Bayer HealthCare, Berlin, Germany) in varying dosages were used to image thrombus deposition and growth within the BFS model against blood flow in real time.

Materials and methods

Experimental flow loop

An acrylic BFS model with dimensions shown in Fig. 1 was used in this study. The upstream diameter was 7.5 mm, while the downstream diameter was 10 mm, resulting in a

Fig. 1 MRI experimental setup for blood recirculation through an acrylic backward facing step model. The inlet and outlet of the flow loop were only used when filling the loop with fluid and were clamped during blood recirculation



step with 2.5 mm in height. The length of the upstream was 200 mm and that of the downstream was 150 mm, which ensured flow to be fully developed at the step region [21].

An experimental flow loop involving the BFS model was constructed (setup is shown in Fig. 1). A peristaltic pump (Cole-Parmer, Vernon Hills, IL, USA) was used to drive fluid through the loop. The pump was chosen to avoid direct contact with fluid within the loop. Approximately, 4 m of Tygon tubing was used, which allowed a loop through the magnet with the BFS model at the isocenter of the actively shielded magnet, and the peristaltic pump placed next to the magnet outside the 5 gauss line. The inlet tubing length was sufficient to attenuate flow pulsatility and the peristaltic flow such that the pulsatility was negligible when entering the BFS model. In addition, possible imaging-related issues (e.g., folding in phase encoding direction) with a second tube in the radiofrequency resonator, when having a loop within the magnet, could be avoided.

Blood collection, preparation, and characterization

Both bovine and human blood were used for this study. Approximately, 450 mL of bovine blood was collected at the Penn State Dairy Farm under IACUC approval. The blood was stored in a blood bag (Jorgensen Laboratories, Loveland, CO) containing 63 mL of citrate phosphate dextrose adenine (CPDA-1). When human blood was used, approximately 450 mL of blood was collected from healthy volunteers at the Penn State Clinical Research Center under IRB approval. The blood was stored in a blood bag (Terumo Corporation, Tokyo, Japan) containing 50 mL of sodium citrate. Both bovine and human blood were stored at room temperature and used for the MRI experiment within 4 h of collection from the respective species. Immediately prior to use, blood was recalcified by mixing a 6.45% b/w calcium chloride (CaCl_2) solution in 1:50 CaCl_2 /blood volume ratio to reverse the effects of the anti-coagulant. The ratio matched the one in Taylor et al. [20].

The following blood properties were measured at room temperature: density, hematocrit, platelet count, and kinematic viscosity (reported in Table 1). The hematocrit was determined using the Autocrit Ultra 3 microcentrifuge (Clay Adams, Franklin Lakes, NJ). The platelet count was obtained

via the hemocytometer. The dynamic viscosity was measured using a cone and plate viscometer, HAAKE RotoVisco 1 (Thermo Scientific™, Horsham, Australia) whereby data collection was controlled by the RehoWin program (Thermo Scientific™, Horsham, Australia). The kinematic viscosity was equal to dynamic viscosity divided by density.

Blood recirculation

The flow loop was initially filled with PBS, which allowed air bubbles to be removed from the system. The PBS was then displaced with recalcified blood. Once the entire loop was filled with blood, blood was circulated within a closed loop for 30 min at room temperature. At the inlet of the BFS model, flow rate was set to be 0.76 L/min, matching the settings in Taylor et al. [20]. At 3, 9, 19, and 29 min of blood recirculation, Gadolinium (Gd, Magnevist) was injected upstream of the model into the flow, 2 meters away from the BFS model (0.75 vol% Gd for the first time and 0.25 vol% afterwards). Magnevist was chosen to be the contrast agent for the current study as it did not disrupt the thrombus stability nor made the thrombus fragile [22]. The amount of injected Gd was determined by preliminary studies, in which different Gd dosages were injected into the flow loop. The dosage that maximized the contrast between thrombus and blood flow was chosen. MRI scans were obtained after 1–2 min of each Gd injection to allow for complete mixing of Gd and blood, and the growing thrombus within the BFS model was imaged at 5, 10, 15, 20, 25, and 30 min of blood recirculation. The timeline of Gd injection and MRI scan performance is shown in Fig. 2. For human and bovine blood studies, blood was collected from different human donors/bovine six times and the loop experiment was performed after each blood collection. Thus, the loop experiments for each species were completed six times to improve data accuracy (i.e., $n=6$ for human blood and $n=6$ for bovine blood).

Magnetic resonance imaging

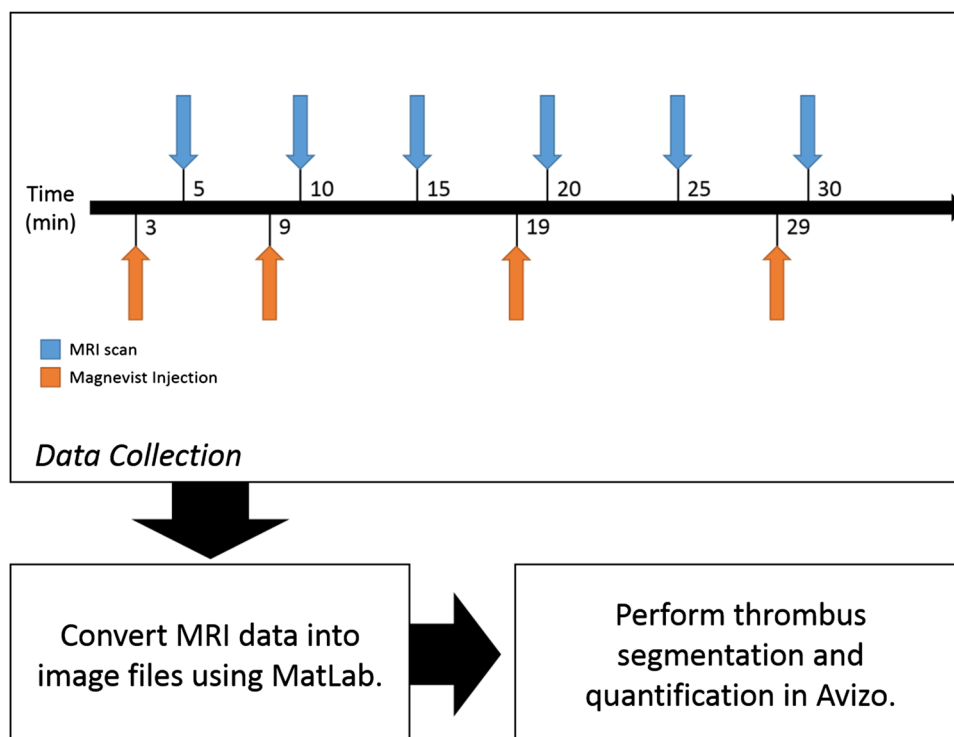
A 7-T preclinical MRI system (BioSpec 70/30, Avance III HD, Bruker Biospin, Billerica, MA) was used for imaging. A three-dimensional flow-compensated gradient echo sequence was used to acquire images of the forming thrombus at the

Table 1 Averaged human and bovine blood properties measured at room temperature, in comparison to those reported in Taylor et al. [20]

	Human blood	Bovine blood	Bovine blood Taylor et al.
Density (g/mL)	1.038 ± 0.002	1.023 ± 0.006	–
Hematocrit (%)	39 ± 1.2	30 ± 1.1	30
Platelet count ($\times 10^6$ platelets/mL)	185 ± 14.7	254 ± 27.9	–
Kinematic viscosity (cSt)	4.4 ± 0.2	3.5 ± 0.3	3.5

The errors represent SEM for the current study ($N=6$)

Fig. 2 Workflow of the experiment



specified time points. With a repetition time of 30 ms, a field of view of $28 \times 11 \times 11$ mm, where the long dimension was aligned with the mainstream flow direction, and a matrix size of $184 \times 72 \times 72$, a spatial resolution of $152 \times 153 \times 153 \mu\text{m}^3$ could be achieved in less than 3 min imaging time. The flip angle was set to be 60° , and the echo time 4.3 ms. Since the thrombus needed to be imaged every 5 min of blood recirculation, the above MRI settings were chosen to create the best contrast between the growing thrombus and the flowing blood with minimal imaging time. Application of Magnevist enhanced the signal-to-noise ratio (SNR) in thrombus, resulting in a ratio of 1.4 ± 0.2 between SNR of thrombus and SNR of blood.

Image reconstruction and segmentation

Magnetic resonance imaging data analysis was performed following the protocol established in Taylor et al. [20]. The MRI data were reconstructed using an in-house Matlab (The Math Works, Inc., Natick, MA) code, in which MRI data converted into image files. Zero filling by a factor of two was applied to improve the image pixel resolution to be $76 \times 76.5 \times 76.5 \mu\text{m}^3$. Image segmentation and data analysis were performed using Avizo (ThermoFisher Scientific, Waltham, MA), which quantified the thrombus size through the following metrics: height, length, volume, and surface area exposed to blood. The MR images were segmented and reconstructed using the modified marching cubes algorithm in Avizo. The thrombus was segmented based on the

contrast established in the MR images, as shown in Fig. 3. The volume and exposed surface area of the thrombus were measured using built-in algorithms provided by Avizo (i.e., the Material Statistics tool). The length was measured by multiplying the total number of slices along the direction of the length with the resolution at that direction. The height was measured via the ruler functionality. The rate of increase was the linear slope of the best-fitted line of the data points. The experimental results were compared to measurements obtained from Taylor et al. [20].

Numerical simulations

To characterize the flow field within the BFS model, numerical simulations, following the method established in Taylor et al. [20], were performed using an open-source CFD package, OpenFOAM (OpenCFD, Ltd, Bracknell, UK). Human and bovine blood flowing through the BFS model were simulated. The Navier–Stokes equations were solved by the pressure implicit with splitting of operator (PISO) algorithm [23], and the velocity and pressure fields were obtained.

The region of interest was a three-dimensional (3D) BFS model, with dimensions shown in Fig. 1. The no-slip velocity condition was imposed at all wall boundaries. At the outlet, the zero Dirichlet boundary condition was applied for pressure (i.e., zero pressure). At all other boundaries, the zero Neumann boundary condition was imposed for velocity and pressure (i.e., zero velocity and pressure gradients). At the inlet, blood flow was assumed to be Newtonian and

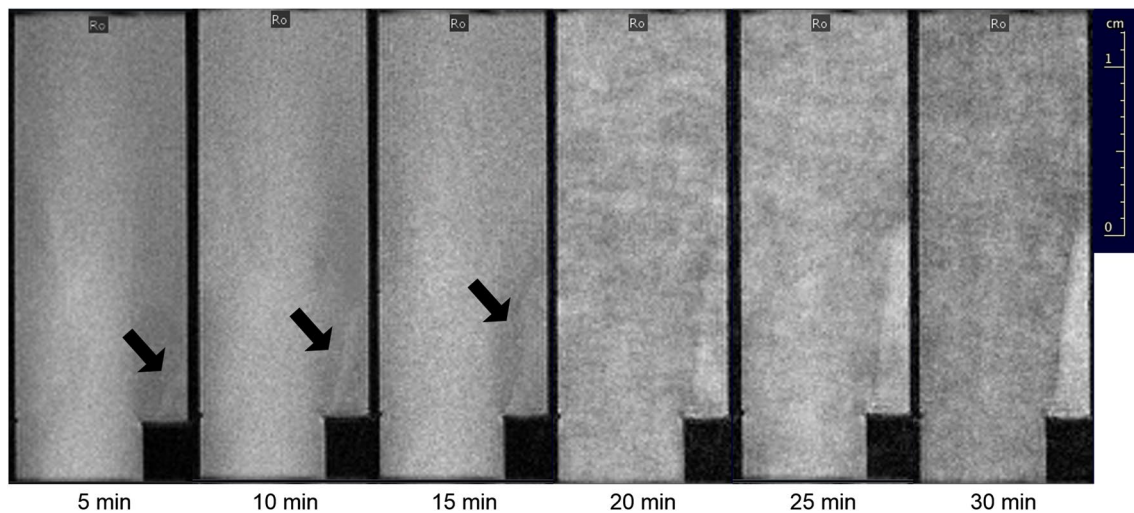


Fig. 3 In vitro magnetic resonance imaging of the thrombus grown at the backward facing step model over blood recirculation time. Human blood flowed from bottom to top. Arrows indicate location of the thrombus from 5 to 15 min. Ro = anterior–posterior direction

steady. The kinematic viscosity was 3.5 cSt for bovine blood and 4.4 cSt for human blood, the asymptotic values measured at room temperature. The mean velocity at the inlet was set to be 0.201 m/s, corresponding to the flow rate of 0.76 L/min.

The computational mesh was composed of uniform cells with an isotropic mesh size of 325 μm in regions away from the walls. In regions near the walls, the isotropic mesh was refined to be 163 μm . As the BFS model was symmetric along the centerline, to reduce the computational cost, only half of the geometry was applied for the simulations, with the centerline plane set as the plane of symmetry. As a result, the 3D geometry was composed of 0.7 million elements. The time step size was chosen to be 0.5 ms for a Courant number (Co) less than 1. In one-dimension, Co is defined as $u * \Delta t / \Delta x$, where u is velocity, Δt is time step size, and Δx is mesh size. A Co less than 1 guaranteed numerical stability [24]. Simulations of blood flowing through the BFS model for 10 s were performed to ensure fully developed flow. The velocity fields resulting from human and bovine blood simulations were compared and analyzed. The flow recirculation region, where the axial velocity becomes negative, was identified.

Results

Magnevist enhanced thrombus imaging

Application of Magnevist enhanced imaging of the thrombus grown within the BFS model. As shown in Fig. 3, the thrombus was already visible in the MRI at 5 min after start of the flow. Continuous addition of Magnevist throughout

blood recirculation further distinguished the thrombus from blood flow.

Flow recirculation region effects

In the MRI study, the thrombus formed under fully developed flow. In the CFD study, blood flowing through the BFS model without thrombus formation was simulated until the flow became fully developed to determine the flow effects. The numerical simulations show that flow recirculation occurred at the step of the BFS model during blood flow (Fig. 4). Length, height, surface area exposed to blood, and volume of the recirculation region were measured and reported in Table 2. As Taylor et al. [20] used bovine blood in their studies as well (Table 1), the resultant recirculation region in this study was of the same sizes. As human blood was more viscous than bovine blood (4.4 ± 0.2 cSt vs. 3.5 ± 0.3 cSt), the resultant recirculation region had a shorter reattachment length (9.75 mm vs. 11.54 mm), which was the distance from flow separation to reattachment, i.e., the distance from the step where the axial velocity changes from negative to positive flow direction. The shorter the reattachment length, the smaller the thrombus formed. By 30 min of flow recirculation, in comparison to bovine blood, human blood resulted in smaller thrombus formation, in terms of the length (13.3 ± 0.6 vs. 18.1 ± 1.3 mm, $p = 0.0072$, one-tailed t test with equal variance based on Levene's test (MatLab)), height (2.3 ± 0.1 vs. 2.6 ± 0.04 mm, $p = 0.0005$), surface area exposed to blood (1.05 ± 0.08 cm², $p = 0.0048$), and volume (0.069 ± 0.004 vs. 0.093 ± 0.007 cm³, $p = 0.003$).

In the experiments, all thrombus deposition and growth occurred at the step of the BFS model, resulting in thrombi

Fig. 4 Velocity fields within the backward facing step model for human and bovine blood experiments. The recirculation region at the step is highlighted by the contour (white lines) and the reattachment length is indicated

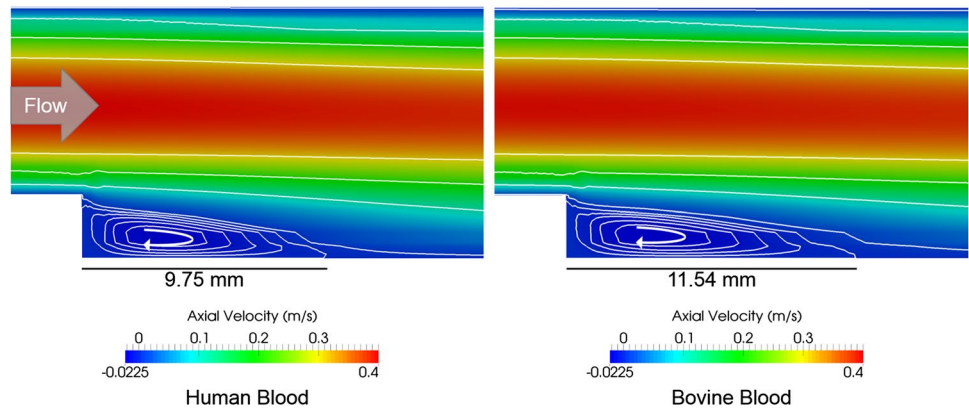


Table 2 Length, height, surface area exposed to blood, and volume of the recirculation region for human and bovine blood experiments

	Human blood	Bovine blood	Bovine blood Taylor et al.
Length (mm)	9.75	11.54	11.54
Height (mm)	2.10	2.14	2.14
Surface area exposed to blood (cm ²)	0.24	0.30	0.30
Volume (cm ³)	0.027	0.032	0.032

The measurements were obtained from numerical simulations

with a triangular ramp shape, regardless of flow recirculation time (Fig. 5), which matched the observations in Taylor et al.

[20]. The thrombi were the widest and thickest at the step corner and became gradually smaller in the flow direction.

Thrombosis quantification

As mentioned before, the size and shape of the recirculation region affected the thrombus formation. To determine the effects of real-time MRI and blood properties other than viscosity, the length, height, surface area exposed to blood, and volume of the thrombus grown within the BFS model over time were normalized by the respective metric of the flow recirculation region (Table 2). For example, the normalized thrombus length, as shown in Fig. 6a, was the ratio between the length of the thrombus and that of the flow recirculation region measured from the CFD simulations. In addition, the

	Human Blood		Bovine Blood		Bovine Blood (Taylor et al.)	
	Side View	Top View	Side View	Top View	Side View	Top View
5 min						
10 min						
15 min						
20 min						
25 min						
30 min						

Fig. 5 Example thrombi grown within the backward facing step model over blood recirculation time, where blood flowed from left to right. Side and top views of the thrombi reconstructed in current study and Taylor et al. [20] are shown for comparison

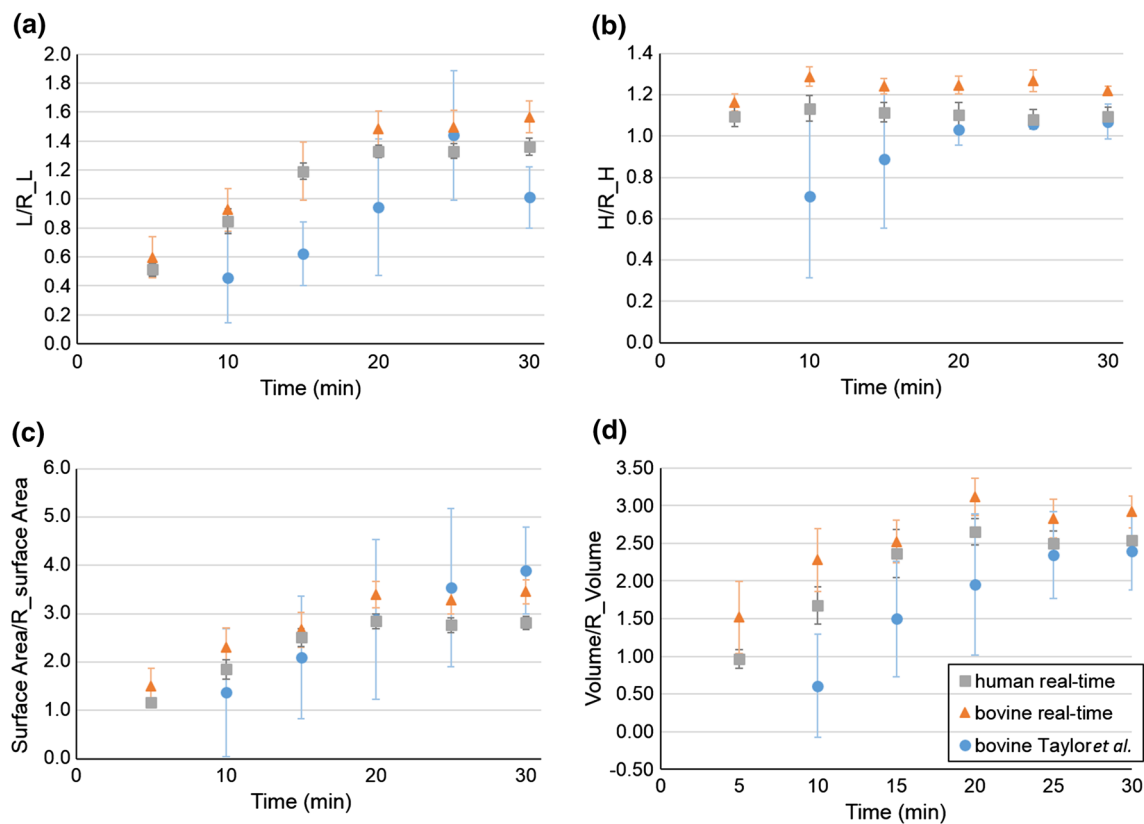


Fig. 6 Quantification of thrombus deposition and growth within the backward facing step model for human and bovine blood experiments, in comparison to measurements from Taylor et al. [20]. The normalized **a** length, **b** height, **c** surface area exposed to blood, and **d** volume of the thrombus grown within the model over blood recirculation time are shown. All metrics were normalized by the respective

rate of increase, the linear slope of the best-fitted line of the data points, was calculated. For the current study, the thrombus sizes stabilized at 20 min and the rate was calculated using data from 5 to 20 min. For Taylor et al. [20], there was a 5-min delay in thrombosis and the thrombus sizes stabilized at 25 min. The rate was calculated from 10 to 25 min.

Both human and bovine blood studies suggested that the normalized thrombus length increased during the first 15 min of blood recirculation and stabilized after 20 min (Fig. 6a). While the normalized thrombi lengths were similar from 5 to 15 min for both studies, with similar rate of increase (0.056 min^{-1} for human blood and 0.058 min^{-1} for bovine blood, with differences less than 5%), the maximum thrombus length resulting from the bovine blood was longer than that of human blood. During the first 20 min, the thrombus lengths from the current study were always longer than measurements from Taylor et al. [20]. However, the rate of increase of the normalized thrombus length was faster in Taylor et al. [20] (0.065 min^{-1}) and the maximum thrombus lengths were approximately the same in both bovine studies.

metric of the flow recirculation region (R) in the model, where the thrombus growth was initiated. E.g. in **a** L/L_R indicates thrombus length normalized by length of the recirculation region. The error bars represent SEM with $N=6$ for the current study and $N=3$ for Taylor et al. [20]

In the current study, the height of the thrombus had reached beyond the flow recirculation region within 5 min, resulting in normalized heights greater than 1 (Fig. 6b). Afterwards, the thrombus height became stable with small fluctuations. While both human and bovine blood studies had stabilized thrombus height at 5 min, the maximum thrombus height of bovine blood was greater than that of human blood. Different from the current study, Taylor et al. [20] resulted in a normalized thrombus height approximately 40% shorter at 10 min. The height increased from 10 to 20 min and became stable after 25 min, reaching the same maximum as that of human blood.

The normalized surface area exposed to blood of the thrombus had similar trends to the normalized length (Fig. 6c). For both human and bovine blood studies, the area increased from 5 to 15 min and stabilized after 20 min. The area of bovine blood was always greater than that of human blood, with a larger maximum. The normalized thrombus area from Taylor et al. [20] kept increasing over flow recirculation time. The areas were smaller than that of bovine

blood from 10 to 20 min but became the largest among all three studies after 25 min.

The thrombus volume was also quantified and plotted over blood recirculation time (Fig. 6d). The figure suggests that for both human and bovine blood, the normalized thrombus volume increased during the first 15 min and stabilized after 20 min. The volume of bovine blood was always greater than that of human blood. In Taylor et al. [20], the normalized thrombus volume increased from 10 to 20 min and stabilized after 25 min, and the values were always lower than those of the current study. As shown in Fig. 6, the standard error of the mean (SEM) resulting from the current study was smaller than that from Taylor et al. [20], which suggests that the current study had less variability when compared to Taylor et al. [20].

To determine the intra-observer variability, the same MRI dataset was analyzed by the same observer three times, in which the thrombus was segmented in Avizo and sizes of the thrombus were measured: the length, height, surface area exposed to blood, and volume. For each metric, the coefficient of variation (CV) was calculated. To determine the inter-observer variability, the same MRI dataset was analyzed by three observers independently. Sizes of the thrombus were measured and CV was calculated for each metric. The results showed that the intra-analysis had a $CV \leq 5\%$ and the inter-analysis had a $CV \leq 10\%$, suggesting that the experiment is repeatable.

Discussions

Magnevist effects

Magnevist is predominantly used as a T1 contrast agent [25]. In other words, it reduces the time the magnetization needs to reach equilibrium magnetization and, therefore, produces a hyperintense signal in the image in areas exposed to the contrast agent. For example, Magnevist can be applied to detect human hepatocellular carcinoma [26]. Preliminary studies have shown that increasing the concentration of Magnevist would reduce not only T1 but also T2 (and therefore T2*; we used a gradient echo sequence that was T2* weighted). The reduction of T2* would lead to a signal loss in the image. In our case, we injected Magnevist at a relative early timepoint to take advantage of the T1 effects of the contrast agent and got more signal from the blood/thrombus than without Magnevist. By adding more Magnevist at the various timepoints, we increased the concentration of Magnevist, which led to reduction of the signal of the blood (T2* reduction effect). The thrombus itself started to appear bright in the images (Fig. 3). By continuing to add Magnevist, we were able to maintain this intensity gradient between blood and thrombus throughout the rest of the experiment.

The loss of signal-to-noise ratio in the blood can be seen in the ‘graininess’ of the blood signal in the later images.

Our imaging method might remind the reader of a technique called time of flight imaging that is usually used for MR angiography (sometimes with support of Magnevist for enhanced contrast [27]). The blood vessels in this technique are, due to the inflow of new, magnetized blood, very well delineated in the image and the stationary, not moving/inflowing tissue is saturated and is showing purposely hardly any signal at all. With our combination of this sequence and the right amounts of Magnevist, we were able to adjust the imaging parameters (especially TR, TE, and the flip angle) in such a way that the delineation of the thrombus was possible throughout the experiment.

Flow recirculation region effects

Because of the presence of flow recirculation within the BFS model, platelet aggregation was promoted at the step region, leading to thrombus formation. All the resultant thrombi had a triangular ramp shape, matching that of the recirculation region. Sizes of the recirculation region were affected by the fluid viscosity when the inlet flow conditions remained the same. Since bovine blood was less viscous than human blood, the Reynolds number (Re) for bovine blood study was higher (490 vs. 388) and the recirculation region was larger, which allowed a larger thrombus to form. The current study measured the length, height, exposed surface area, and volume of the flow recirculation region through the CFD simulations. To obtain real-time measurements, future MRI studies can be performed in which 4D flow MRI or the flow map imaging technique can be applied to obtain the velocity field within the BFS model.

Blood properties effects

Both human and bovine blood studies showed that the normalized thrombus sizes increased during the first 15 min of blood recirculation and stabilized after 20 min (Fig. 6). The thrombus sizes no longer changed at a later time because the thrombus formed when a finite amount of blood was recirculating within a closed loop, where the amount of platelets and coagulation factors were finite. When the species contributing to the thrombosis pathway were all consumed, the thrombus growth ceased, and the thrombus sizes became stable. Another potential cause for the halt of thrombus growth was the fact that the grown thrombus occupied the entire recirculation region. However, Fig. 6c and d suggest that in all three cases, the thrombus did not stop growing until the thrombus exposed surface area and volume were approximately three times that of the recirculation region. If occupying the recirculation region led to asymptotic thrombus growth, the thrombus would have asymptotic sizes similar

to that of the recirculation region, instead of being much greater. Therefore, recirculating blood in a closed loop was the reason for stabilized thrombosis.

From 5 to 15 min, the thrombus from human blood reached the asymptotic shape faster than that of bovine blood, with a greater rate of increase in normalized thrombus volume (Fig. 6d, 0.12 min^{-1} for human blood and 0.10 min^{-1} for bovine blood). The reason was that human blood had a higher hematocrit (39% vs. 30%, corresponding to the higher viscosity). Studies have shown that the platelet concentrations in the near-wall region (platelet margination) increased with hematocrit, which promoted platelet aggregation at the step region [28, 29]. In addition, red blood cells (RBCs) elevated activation of platelet $\alpha_{\text{IIb}}\beta_3$ integrin receptors and expression of P-selectin in presence of agonists such as thrombin, both of which promoted platelet aggregation [30, 31]. For human blood, with a higher hematocrit, more RBCs were available, and platelet margination and platelet aggregation were enhanced, allowing the thrombus to grow more quickly at the step. As a result, the increase in hematocrit increased the rate of thrombus volume, and, therefore, the rate of thrombus growth, which has been observed in other studies [32, 33].

When the thrombus sizes were normalized by those of the respective blood recirculation region, bovine blood still resulted in larger thrombus formation in comparison to human blood by 30 min of blood recirculation (Fig. 6). The normalized thrombus surface area exposed to blood and the normalized height of bovine blood were significantly greater than that of human blood at 30 min, with $p < 0.05$. A higher platelet count in bovine blood ($254 \text{ vs. } 185 \times 10^6$ platelets/mL) was associated with the larger thrombus formation. Studies have shown that increase in platelet count was correlated with higher risk of thrombosis [34–36]. With more platelets available, platelet–platelet interactions were enhanced, platelet activities with coagulation factors were promoted, and more chemicals were released from platelets, all of which contributed to the larger thrombus formation [34]. As mentioned previously, RBCs promoted activation of platelet $\alpha_{\text{IIb}}\beta_3$ integrin receptors, which bound fibrinogen and caused thrombus retraction [37]. Since human blood had a higher hematocrit, and therefore more RBCs per volume, the thrombus retracted more, resulting in smaller sizes.

Comparison to previous studies

The current study is novel as it has, to the best of our knowledge, only been performed by our group. However, Goodman et al. [38] has applied scanning electron microscopy and video microscopy to detect thrombus deposition in a channel with expansions and contractions. The study observed thrombus deposition at the flow recirculation

region induced by the channel expansions, which agreed with our observations.

For the Taylor et al. [20] study, there was a 5-min delay in thrombus deposition and growth, and the thrombus sizes were generally smaller when compared to the current bovine blood study, though both studies used bovine blood with similar properties ($\text{Re} = 490$) and had MRI scans with similar resolution. The difference in experimental design led to different results. In Taylor et al. [20], images of the thrombus were obtained while the thrombus was in contrast against stationary PBS, instead of flowing blood. A numerical study has shown that within the thrombus grown at the step, there were more platelets aggregated in region closer to the step corner than near the thrombus surface exposed to flow [11]. As a result, the thrombus was more porous and less rigid near the surface. In addition, thrombus breakdown associated with inhibitors (e.g., anti-thrombin III, APC) and high shear stress occurred during thrombosis [13]. The thrombus grew at the step when thrombosis outperformed the breakdown process. However, when blood was replaced with PBS for imaging, the thrombus formed no longer received supplies of platelets and coagulation factors from the mainstream and stopped growing, while experiencing additional shear induced by the fluid replacement process. In this case, thrombus breakdown outperformed the thrombosis reactions and the thrombus surface region, which was less rigid, became more susceptible to the breakdown, resulting in a smaller thrombus. In addition, the fluid replacement affected the resultant thrombus topology, smoothing the edges and surface of the thrombus. As shown in Fig. 5, the thrombi from the current bovine study had a rougher surface and wider region toward the tail.

The current study is the first one applying flow-compensated MRI and Magnevist to visualize thrombus formation against blood flow in a BFS model, which improved the experimental design developed in Taylor et al. [20] and provided additional experimental data for device-induced thrombosis. As discussed earlier, the flow fields and blood properties (i.e., hematocrit and platelet count) affected thrombosis, which should be considered and coupled when developing computational thrombosis models. The data collected in Taylor et al. [20] have been used to validate thrombosis models in multiple occasions [11, 14]. The current study has provided additional data for quantification of thrombosis within a device by considering how flow alters the growth. Future thrombosis models can be applied to simulate thrombus deposition and growth induced by a BFS model, and compare the simulation results to the experimental data provided for model validation. The validated computational models become useful when evaluating the risk of thrombosis for a device, promoting design optimization of the device before bench top, animal, and clinical studies.

Conclusions

For the first time, the current study used real-time contrast agent-supported MR imaging of thrombus deposition and growth within a sudden expansion. Results showed that in studies using human and bovine blood, thrombus sizes increased during the first 15 min of blood recirculation and reached asymptotic values after 20 min. Thrombus growth was affected by the flow recirculation region and blood properties. The larger the flow recirculation region, the larger the thrombus formed. Increase in hematocrit increased the rate of thrombus growth and promoted thrombus retraction, while higher platelet count was associated with larger thrombus formation. This study provides more experimental data for thrombosis within a device, which is valuable for validation of computational thrombosis models.

Acknowledgements This research was supported, in part, by NIH Grant T32GM108563 and HL136369.

Author contributions LY: study conception and design, acquisition of data, analysis and interpretation of data, drafting of manuscript, critical revision. TN: study conception and design, critical revision. KBM: study conception and design, analysis and interpretation of data, drafting of manuscript, critical revision

Compliance with ethical standards

Conflict of interest The authors declare that they have no conflict of interest.

Ethics approval All applicable international, national, and/or institutional guidelines for the care and use of animals were followed. The study was approved by the Penn State University IACUC (PRAMS200946269). All procedures performed in studies involving human participants were in accordance with the ethical standards of the institutional and/or national research committee and with the 1964 Helsinki declaration and its later amendments or comparable ethical standards. The study was approved by the Penn State University IRB (STUDY00009649).

Informed consent Informed consent was obtained from all individual participants included in the study.

References

- Benjamin EJ, Blaha MJ, Chiuve SE, Cushman M, Das SR, Deo R, De Ferranti SD, Floyd J, Fornage M, Gillespie C, Isasi CR, Jimenez MC, Jordan LC, Judd SE, Lackland D, Lichtman JH, Lisabeth L, Liu S, Longenecker CT, MacKey RH, Matsushita K, Mozaffarian D, Mussolino ME, Nasir K, Neumar RW, Palaniappan L, Pandey DK, Thiagarajan RR, Reeves MJ, Ritchey M, Rodriguez CJ, Roth GA, Rosamond WD, Sasson C, Towfghi A, Tsao CW, Turner MB, Virani SS, Voeks JH, Willey JZ, Wilkins JT, Wu JHY, Alger HM, Wong SS, Muntner P (2017) Heart disease and stroke statistics—2017 update: a report from the American Heart Association. *Circulation* 135:e146–e603
- Kirklin JK, Naftel DC, Kormos RL, Pagani FD, Myers SL, Stevenson LW, Acker MA, Goldstein DL, Silvestry SC, Milano CA, Baldwin JT, Pinney S, Rame JE, Miller MA (2014) Interagency Registry for Mechanically Assisted Circulatory Support (INTERMACS) analysis of pump thrombosis in the HeartMate II left ventricular assist device. *J Hear Lung Transplant* 33:12–22
- Dürreman N, Pellerin M, Bouchard D, Hébert Y, Cartier R, Perault LP, Basmadjian A, Carrier M (2004) Prosthetic valve thrombosis: twenty-year experience at the Montreal Heart Institute. *J Thorac Cardiovasc Surg* 127:1388–1392
- Nobili M, Sheriff J, Morbiducci U, Redaelli A, Bluestein D (2008) Platelet activation due to hemodynamic shear stresses: damage accumulation model and comparison to in vitro measurements. *ASAIO J* 54:64–72
- Navitsky MA, Deutsch S, Manning KB (2013) A thrombus susceptibility comparison of two pulsatile Penn state 50 cc left ventricular assist device designs. *Ann Biomed Eng* 41:4–16
- Vogler EA, Siedlecki CA (2009) Contact activation of blood-plasma coagulation. *Biomaterials* 30:1857–1869
- Chesnutt JKW, Han HC (2016) Computational simulation of platelet interactions in the initiation of stent thrombosis due to stent malapposition. *Phys Biol* 13:016001
- Ou C, Huang W, Yuen MMF (2017) A computational model based on fibrin accumulation for the prediction of stasis thrombosis following flow-diverting treatment in cerebral aneurysms. *Med Biol Eng Comput* 55:89–99
- Topper SR, Navitsky MA, Medvitz RB, Paterson EG, Siedlecki CA, Slattery MJ, Deutsch S, Rosenberg G, Manning KB (2014) The use of fluid mechanics to predict regions of microscopic thrombus formation in pulsatile VADs. *Cardiovasc Eng Technol* 5:54–69
- Chivukula VK, Beckman JA, Prisco AR, Dardas T, Lin S, Smith JW, Mokadam NA, Aliseda A, Mahr C (2018) Left ventricular assist device inflow cannula angle and thrombosis risk. *Circ Heart Fail*. <https://doi.org/10.1161/CIRCHEARTFAILURE.117.004325>
- Taylor JO, Meyer RS, Deutsch S, Manning KB (2016) Development of a computational model for macroscopic predictions of device-induced thrombosis. *Biomech Model Mechanobiol* 15:1713–1731
- Taylor JO, Yang L, Deutsch S, Manning KB (2017) Development of a platelet adhesion transport equation for a computational thrombosis model. *J Biomech* 50:114–120
- Fogelson AL, Guy RD (2008) Immersed-boundary-type models of intravascular platelet aggregation. *Comput Methods Appl Mech Eng* 197:2087–2104
- Menichini C, Xu XY (2016) Mathematical modeling of thrombus formation in idealized models of aortic dissection: initial findings and potential applications. *J Math Biol* 73:1205–1226
- Wu WT, Jamiolkowski MA, Wagner WR, Aubry N, Massoudi M, Antaki JF (2017) Multi-constituent simulation of thrombus deposition. *Sci Rep*. <https://doi.org/10.1038/srep42720>
- Méndez Rojano R, Mendez S, Nicoud F (2018) Introducing the pro-coagulant contact system in the numerical assessment of device-related thrombosis. *Biomech Model Mechanobiol* 17:815–826
- Ihn YK, Jung WS, Hwang SS (2013) The value of T2*-weighted gradient-echo MRI for the diagnosis of cerebral venous sinus thrombosis. *Clin Imaging* 37:446–450
- Kluge A, Mueller C, Strunk J, Lange U, Bachmann G (2006) Experience in 207 combined MRI examinations for acute pulmonary embolism and deep vein thrombosis. *Am J Roentgenol* 186:1686–1696
- Overoye-Chan K, Koerner S, Looby RJ, Kolodziej AF, Zech SG, Deng Q, Chasse JM, McMurry TJ, Caravan P (2008) EP-2104R: A fibrin-specific gadolinium-based MRI contrast agent for detection of thrombus. *J Am Chem Soc* 130:6025–6039

20. Taylor JO, Witmer KP, Neuberger T, Craven BA, Meyer RS, Deutsch S, Manning KB (2014) In vitro quantification of time dependent thrombus size using magnetic resonance imaging and computational simulations of thrombus surface shear stresses. *J Biomech Eng*. <https://doi.org/10.1115/1.4027613>
21. Bergman TL, Lavine AS (2018) *Fundamentals of heat and mass transfer*, 8th edn. Wiley, Hoboken
22. Walvick RP, Brátane BT, Henninger N, Sicard KM, Bouley J, Yu Z, Lo E, Wang X, Fisher M (2011) Visualization of clot lysis in a rat embolic stroke model: application to comparative lytic efficacy. *Stroke* 42:1110–1115
23. Ferziger JH, Perić M (2002) *Computational methods for fluid dynamics*, 3rd ed. *Comput Methods Fluid Dyn*. <https://doi.org/10.1007/978-3-642-56026-2>
24. Courant R, Friedrichs K, Lewy H (1928) Über die partiellen Differenzgleichungen der mathematischen Physik. *Math Ann* 100:32–74
25. Ibrahim MA, Hazhirkarzar B, Dublin AB (2018) *Magnetic resonance imaging (MRI)*. StatPearls Publishing, Gadolinium
26. Liu Y, Chen Z, Liu C, Yu D, Lu Z, Zhang N (2011) Gadolinium-loaded polymeric nanoparticles modified with Anti-VEGF as multifunctional MRI contrast agents for the diagnosis of liver cancer. *Biomaterials* 32:5167–5176
27. Goyen M, Lauenstein TC, Herborn CU, Debatin JF, Bosk S, Ruehm SG (2001) 0.5 M Gd chelate (Magnevist®) versus 1.0 M Gd chelate (Gadovist®): dose-independent effect on image quality of pelvic three-dimensional MR-angiography. *J Magn Reson Imaging* 14:602–607
28. Aarts PAMM, Van den Broek SAT, Prins GW, Kuiken GDC, Sixma JJ, Heethaar RM (1988) Blood platelets are concentrated near the wall and red blood cells, in the center in flowing blood. *Arteriosclerosis*. <https://doi.org/10.1161/01.atv.8.6.819>
29. Zhao R, Kameneva MV, Antaki JF (2007) Investigation of platelet margination phenomena at elevated shear stress. IOS Press, Amsterdam
30. Silvain J, Abtan J, Kerneis M, Martin R, Finzi J, Vignalou JB, Barthélémy O, O'Connor SA, Luyt CE, Brechot N, Mercadier A, Brugier D, Galier S, Collet JP, Chastre J, Montalescot G (2014) Impact of red blood cell transfusion on platelet aggregation and inflammatory response in anemic coronary and noncoronary patients: the TRANSFUSION-2 study (Impact of transfusion of red blood cell on platelet activation and aggregation studied with flow c. *J Am Coll Cardiol* 63:1289–1296
31. Vallés J, Teresa Santos M, Aznar J, Martínez M, Moscardó A, Piñón M, Johan Broekman M, Marcus AJ (2002) Platelet-erythrocyte interactions enhance α Ib β 3 integrin receptor activation and P-selectin expression during platelet recruitment: down-regulation by aspirin ex vivo. *Blood* 99:3978–3984
32. Walton BL, Lehmann M, Skorczewski T, Holle LA, Beckman JD, Cribb JA, Mooberry MJ, Wufsus AR, Cooley BC, Homeister JW, Pawlinski R, Falvo MR, Key NS, Fogelson AL, Neeves KB, Wolberg AS (2017) Elevated hematocrit enhances platelet accumulation following vascular injury. *Blood* 129:2537–2546
33. Ouaknine-Orlando B, Samama CM, Riou B, Bonnin P, Guillosson JJ, Beaumont JL, Coriat P (1999) Role of the hematocrit in a rabbit model of arterial thrombosis and bleeding. *Anesthesiology* 90:1454–1461
34. Jensen MK, Brown PDN, Lund BV, Nielsen OJ, Hasselbalch HC (2001) Increased circulating platelet-leukocyte aggregates in myeloproliferative disorders is correlated to previous thrombosis, platelet activation and platelet count. *Eur J Haematol* 66:143–151
35. Simanek R, Vormittag R, Ay C, Alguel G, Dunkler D, Schwarzwinger I, Steger G, Jaeger U, Zielinski C, Pabinger I (2010) High platelet count associated with venous thromboembolism in cancer patients: results from the Vienna Cancer and Thrombosis Study (CATS). *J Thromb Haemost* 8:114–120
36. Khorana A, Kuderer NM, Culakova E, Lyman GH, Francis CW (2008) Development and validation of a predictive model for chemotherapy-associated thrombosis. *Blood* 111:4902–4907
37. Rooney MM, Parise LV, Lord ST (1996) Dissecting clot retraction and platelet aggregation: clot retraction does not require an intact fibrinogen γ chain C terminus. *J Biol Chem* 271:8553–8555
38. Goodman PD, Barlow ET, Crapo PM, Mohammad SF, Solen KA (2005) Computational model of device-induced thrombosis and thromboembolism. *Ann Biomed Eng* 33:780–797

Publisher's Note Springer Nature remains neutral with regard to jurisdictional claims in published maps and institutional affiliations.